applied sciences

MDPI

Article

Advanced Scheme to Generate MHz, Fully Coherent FEL Pulses at nm Wavelength

Georgia Paraskaki [1], Sven Ackermann [1], Bart Faatz [2], Gianluca Geloni [3,*], Tino Lang [1], Fabian Pannek [4], Lucas Schaper [1] and Johann Zemella [1]

[1] Deutsches Elektronen-Synchrotron DESY, Notkestraße 85, 22607 Hamburg, Germany; georgia.paraskaki@desy.de (G.P.); sven.ackermann@desy.de (S.A.); tino.lang@desy.de (T.L.); lucas.schaper@desy.de (L.S.); johann.zemella@desy.de (J.Z.)
[2] Shanghai Advanced Research Institute, Chinese Academy of Sciences, Haike Road 99, Shanghai 201210, China; faatzbart@sari.ac.cn
[3] European XFEL, Holzkoppel 4, 22869 Schenefeld, Germany
[4] Institute for Experimental Physics, University of Hamburg, Luruper Chaussee 149, 22761 Hamburg, Germany; fabian.pannek@desy.de
* Correspondence: gianluca.geloni@xfel.eu

Abstract: Current FEL development efforts aim at improving the control of coherence at high repetition rate while keeping the wavelength tunability. Seeding schemes, like HGHG and EEHG, allow for the generation of fully coherent FEL pulses, but the powerful external seed laser required limits the repetition rate that can be achieved. In turn, this impacts the average brightness and the amount of statistics that experiments can do. In order to solve this issue, here we take a unique approach and discuss the use of one or more optical cavities to seed the electron bunches accelerated in a superconducting linac to modulate their energy. Like standard seeding schemes, the cavity is followed by a dispersive section, which manipulates the longitudinal phase space of the electron bunches, inducing longitudinal density modulations with high harmonic content that undergo the FEL process in an amplifier placed downstream. We will discuss technical requirements for implementing these setups and their operation range based on numerical simulations.

Keywords: seeded FEL; oscillator; amplifier; high repetition rate

Citation: Paraskaki, G.; Ackermann, S.; Faatz, B.; Geloni, G.; Lang, T.; Pannek, F.; Schaper, L.; Zemella, J. Advanced Scheme to Generate MHz, Fully Coherent FEL Pulses at nm Wavelength. *Appl. Sci.* **2021**, *11*, 6058. https://doi.org/10.3390/app11136058

Academic Editors: Giuseppe Dattoli, Alessandro Curcio and Danilo Giulietti

Received: 25 May 2021
Accepted: 19 June 2021
Published: 29 June 2021

1. Introduction

Free-electron lasers (FELs) have been making enormous improvements during the past decades, delivering high-brightness radiation to users all over the world at wavelengths from mm to hard x-rays, covering a wide range of experiments. At the same time, many experiments, for instance, those that depend on spectroscopic techniques to resolve electronic structure, require full coherence and high statistics, which can only be fulfilled with fully coherent radiation at high repetition rate. These two requirements are becoming important for scientific applications and are driving new FEL developments. Currently, superconducting accelerators are capable of providing thousands of bunches per second at MHz repetition rate. This potential is currently exploited in self-amplified spontaneous emission (SASE) mode [1]. However, in this case, the FEL process starts from random fluctuations of the electron beam charge density distribution [2] leading to a limited temporal coherence, which impacts the peak brightness. The longitudinal coherence can be improved by self-seeding [3,4] and single-mode [5,6] lasing schemes which are based on the SASE process. As a consequence, the stochastic nature of SASE is imprinted on the final FEL pulse as intensity fluctuations even though improved longitudinal coherence is achieved.

At wavelengths in the nanometer range and longer, alternatives to generate fully coherent radiation are based on external seeding. In this case, a seed laser of typically

several tens MW of power is used to prepare an initial signal for a final FEL amplifier, usually tuned at a harmonic of its wavelength, thus imprinting its coherence properties upon the output FEL pulse. Many interesting experiments and methods are allowed due to the unique properties of seed radiation [7–10]. Two chief examples of external seeding schemes are the high-gain harmonic generation (HGHG) [11,12] and the echo-enabled harmonic generation (EEHG) [13–15]. As the harmonic conversion of seeding schemes is limited, it is advantageous to use short wavelength seed lasers. Currently, ultraviolet (UV) seed lasers are the most suitable candidates for such setups [14–16]. However, the requirements put on these laser systems in terms of peak power limit their repetition rate, which is usually in the kHz regime. As seeded radiation pulses can be generated at a maximum repetition rate defined by the seed laser repetition rate, not all electron bunches generated in superconducting accelerators can be seeded. This leads to high peak brightness FEL pulses, but limited average flux, in contrast to the number of electron bunches available. In order to address this limitation, alternatives have been recently studied to increase the repetition rate of seeding schemes by reducing the seed laser power requirements [17,18], and in this paper, we propose an oscillator–amplifier setup.

Here, we review and further discuss a scheme which can generate FEL pulses of both high peak brightness, compared to SASE, and of high average flux compared to standard seeding schemes, by generating high repetition rate seeded radiation pulses [19–22]. In this scheme, an FEL oscillator is employed and acts as a feedback system which recirculates a seed pulse, and seeds the electron bunches at high repetition rate. In this case, one may either use a low repetition rate seed laser, or start from shot noise. Starting from shot noise lets us be independent of seed laser systems both in terms of repetition rate and wavelength. Oscillator FELs are a well-studied topic, and their technology has been established for a long time. There is a wide range of oscillator FELs that were operated during the past decades, and detailed simulation studies were performed almost two decades ago [23–25]. These studies led, more recently, to the development of other ideas such as XFELOs [26] and Regenerative Amplifier Free-Electron Lasers (RAFELs) [27–30] (high-gain oscillators). Both these schemes aim at Angstrom radiation with Bragg crystals instead of conventional mirrors, and no harmonic conversion is used. However, at wavelengths in the nanometer range, where crystal optics cannot be used, mirror technology strongly limits the generation of wavelengths below the 190 nm demonstrated at ELETTRA [31]. In order to reach shorter wavelengths, one can exploit a resonator at a longer wavelength, together with harmonic conversion. Such cascades have been proposed in [32–35]. Earlier work on resonators in the EUV regime can be found in [36].

An overview of the seeding schemes that can employ an oscillator to increase the repetition rate of the FEL radiation is given in Section 2, together with comments on its implementation in continuous wave and burst-mode accelerators. Considerations on the implementation of a resonator and a simple model which can be used for its design are provided in Section 3. In Section 4, we introduce the methods used in simulations for power gain control in the cavity, when the start-up of the FEL process is based on random fluctuations of the initial electron beam distribution. In Section 5, we compare these results to the case of an oscillator where the start-up of the FEL process is based on a low repetition rate external seed laser, to the case of standard single-pass seeding, and to SASE simulations.

2. Overview of Methods

2.1. Employing an Oscillator in Standard Seeding Schemes

In this section, we review different schemes that can be implemented with an oscillator in order to provide high repetition rate seed pulses. In standard seeding techniques, an external seed laser is used to modulate the energy of the electron beam as a result of their interaction along an undulator (modulator). In this case, one seed laser pulse needs to be injected for each electron bunch. The purpose of adding an optical cavity to a seeding scheme is to replace the need for an external seed laser, because the cavity can recirculate a

radiation pulse and maintain its peak power and pulse properties. In this case, in addition to the energy modulation process which happens along the modulator, an amplification process must also occur. This is important because the power gain is used to compensate for unavoidable cavity losses. Here, we define as net gain the difference between the peak power at the beginning of a pass n + 1 and the peak power at the beginning of pass n, divided by the peak power at pass n. If the power gain compensates exactly for the losses and the net gain is zero, the peak power per pass remains constant as long as the pulse properties remain stable. In this way, the seed pulse is reproducible and can support seeding schemes at high repetition rates.

In this paper we consider two approaches to generate and store a seed laser pulse in cavity.

1. An oscillator-FEL starting with an external seed laser pulse. An external seed laser initiates the modulation of the first electron bunch and the bunch amplifies the seed pulse to compensate for the power losses in the cavity. The optical cavity feeds back the seed pulse which is used to modulate the following bunches. The shortest wavelength of the modulator is determined by the low repetition rate seed laser source and by the mirror availability.
2. An oscillator-FEL starting from shot-noise. An electron bunch generates radiation along the modulator, which is amplified with the number of passes. This process can be divided into two phases. The "build-up regime", where the net gain per pass needs to be positive to build up the peak power required for seeding, and the "steady-state regime" where the net gain needs to go back to zero so that the resonator losses are equal to the power gain. In order to transition between these two phases, an active control on the gain per pass is required. In addition, starting from noise means that a SASE spectrum is generated. This needs to be monochromatized. In this case, the shortest wavelength of the modulator is determined by the mirror availability.

In the following, we consider the implementation of an oscillator-based FEL in support to HGHG and EEHG seeding schemes in order to further extend the tuning range to shorter wavelength and higher repetition rate.

2.1.1. High-Gain Harmonic Generation (HGHG)

HGHG is a method to achieve fully coherent and stable seeded radiation in high-gain FELs and was introduced in [11]. The components needed are a modulator, a seed laser resonant to the wavelength of the modulator, a dispersive section, and an FEL amplifier tuned at a harmonic of the seed laser wavelength. The seed laser is overlapped with the electron bunch in the modulator, and their interaction results in a longitudinal sinusoidal energy modulation along the electron bunch with the periodicity of the resonant wavelength. In the dispersive section placed downstream, the energy modulation is converted into density modulation that includes relevant harmonic content. The dispersive section is characterized by the R_{56} matrix element of the transfer matrix, which describes the evolution of the 6-D phase space (x, x', y, y',δ_γ, z) of the electrons. The R_{56} is closely related with the presence of longitudinal dispersion. When a correlation between the longitudinal position (z) and a relative energy offset (δ_γ) is established in the modulator, it is possible to choose an R_{56} to rotate the longitudinal phase space, and convert the energy modulation into longitudinal density modulation. The same matrix element is responsible for the so called bunch compression in accelerators, where we exploit an electron beam with an energy-longitudinal position correlation (electron beam energy chirp) to compress it longitudinally and increase its peak current. After the dispersive section, the bunched electron beam then enters the amplifier and emits coherent radiation. In the case of an HGHG oscillator-amplifier, an optical cavity which encloses the modulator is added as shown in Figure 1. Instead of injecting a seed laser pulse for each consecutive electron bunch, the optical cavity stores a radiation pulse which acts as a seed laser source. Because, as discussed above, a certain amount of power gain is required at each pass, the modulator is longer than in a conventional HGHG scheme.

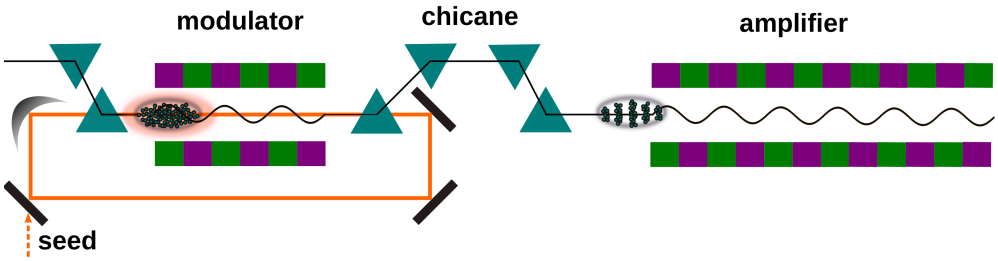

Figure 1. In an oscillator-based HGHG scheme, an optical cavity is added and encloses the modulator. The optical cavity acts as a feedback system which maintains the peak power of the stored radiation field and, under perfect synchronism, this field is used to seed consecutive electron bunches arriving from the linac upstream the cavity. Note that in reality, the optical cavity design will be more complex than this simplified sketch.

2.1.2. Echo-Enabled Harmonic Generation (EEHG)

HGHG schemes are characterized by a limited up-frequency conversion efficiency due to the fact that the nth harmonic requires the energy modulation to be n times larger than the slice energy spread to maximize the bunching. This is typically limiting the conversion to $n = 15$ and critically depends on the energy spread [37]. The EEHG scheme [13–15] was proposed to overcome this limitation, achieve higher harmonics and, thus, shorter wavelengths. In this scheme, there are two seed lasers with two modulators, two dispersive sections, and one radiator. The first modulator and seed laser are used to induce an energy modulation, and then the first dispersive section, which has a large longitudinal dispersion, shreds the longitudinal phase space of the electron beam creating thin energy bands. Each of these bands has a lower energy spread than the initial one, and this way a lower energy modulation is required in the second modulator compared to HGHG. The second dispersive section is weaker and compresses the energy bands. Similarly to what happens in HGHG, it converts the energy modulation from the second modulator into a density modulation, which in this case can have higher harmonic content.

In a regular single-pass EEHG, two modulators and two seed lasers are needed. In order to convert the classic scheme to a high repetition rate cavity-FEL, one possibility is to include two cavities, one for each modulator. In the case of two cavities, the wavelength can be chosen independently and the high repetition rate is secured. Another solution is to feed one modulator with an external seed laser and place the other modulator in a cavity. In this case, the repetition rate of the external seed laser source determines the overall repetition rate. This seed laser should have a longer wavelength which is at present already available at high repetition rate. Then, the other modulator which is enclosed in the optical cavity is resonant to a shorter wavelength.

It is important to investigate if it is more advantageous to have the shortest wavelength at the first or the second modulator. We study the specific case of a combination of two seed laser wavelengths of 300 nm and 50 nm by using an electron beam with a nominal energy of 1.35 GeV, energy spread of 120 keV, and energy modulation amplitudes of $A_1 = 3$ and $A_2 = 5$ times the energy spread in the first and second modulator, respectively. These parameters fit the choices of the FLASH2020+ project [38]. The resulting maximum bunching factor b [13] for final wavelengths between 2 nm and 6 nm is shown in Figure 2a. Using a seed with a wavelength of 50 nm in the first modulator and 300 nm in the second modulator is not beneficial in terms of bunching compared to the classic scheme with two seed lasers with a wavelength of 300 nm, whereas much higher bunching can be achieved by utilizing the shorter seed in the second modulator. Both 50 nm configurations drastically reduce the required longitudinal dispersion of the first chicane, as can be seen in Figure 2b. As the second chicane converts the energy modulation from the second modulator, a seed wavelength of 50 nm in this modulator results in an approximately six times smaller optimum dispersive strength than the one needed for a 300 nm seed.

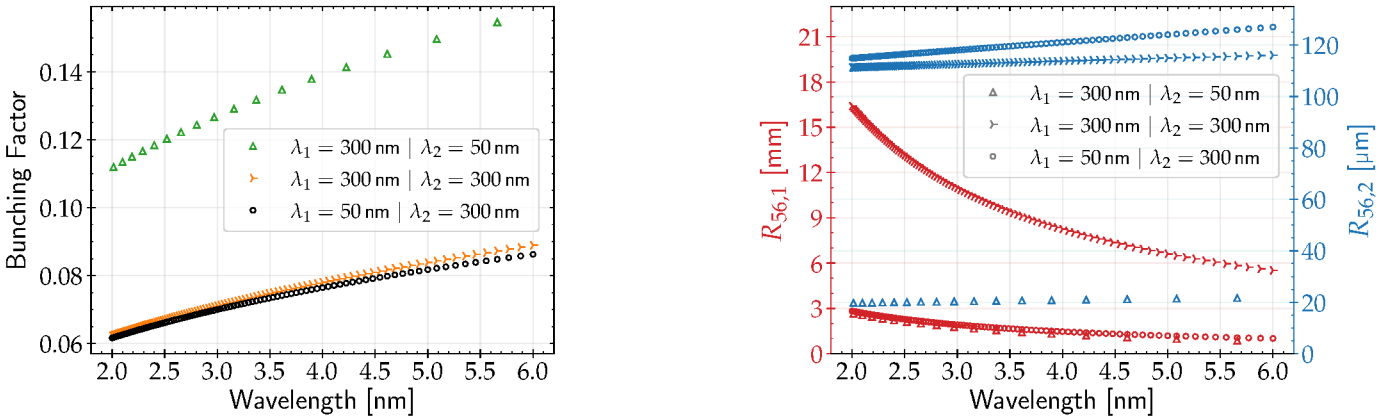

(**a**) (**b**)

Figure 2. (**a**) Maximum bunching factor for different combinations of seed laser wavelengths. (**b**) Optimum setup of the chicanes to maximize the bunching factor. The working point resulting in a lower $R_{56,1}$ is shown for each configuration.

A tunable seed around 50 nm in the second modulator would allow to overcome the limitations of the wavelength separation of the harmonics and provide access to a continuous wavelength range and high bunching. For example, a final target wavelength of 4 nm with more than 13% bunching could be achieved either by a 47.4 nm or a 51.3 nm seed. The preferred setup with the second modulator enclosed in a cavity and thus being resonant to a shorter seed is shown in Figure 3. As a final remark, we note that one cavity could be employed for both modulators, which would be preferred in terms of cavity length requirements. However, in this case, the peak power of the radiation cannot be tuned independently at the two modulators which is an important aspect of the optimization of EEHG.

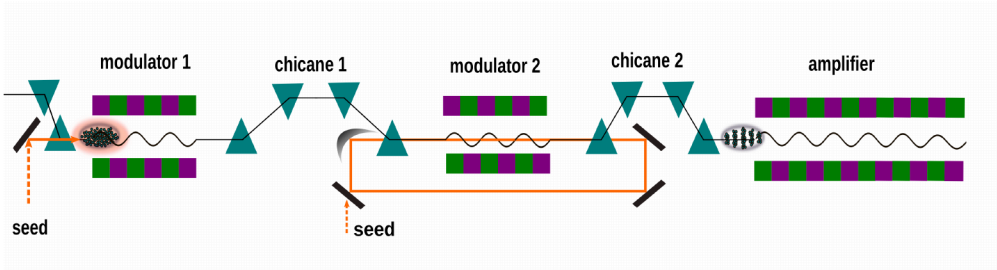

Figure 3. In an oscillator-based EEHG scheme, one or two optical cavities can be attached. In this figure, the first modulation occurs with a conventional external seed laser, while the second energy modulation is achieved by employing an optical cavity around the second modulator. The optical cavity is fed by a seed laser and maintains its properties in order to seed consecutive electron bunches.

To demonstrate the feasibility of the proposed EEHG configuration, a single-pass full simulation with the FEL code Genesis 1.3 [39] is carried out. The wavelengths of the first and the second seed laser are 300 nm and 50 nm, respectively. The electron beam parameters are the same as those used in the already presented analytical calculations above, and in addition, the normalized emittance is 0.6 mm mrad, the electron bunch length is 314 fs full width at half max (FWHM), and the current profile is Gaussian with a peak of 500 A. The duration of the Gaussian seed laser pulses is set to 150 fs and 50 fs FWHM for the first and second seed laser, respectively. The simulation is optimized for an output wavelength of 2.013 nm with longitudinal dispersions of $R_{56,1} = 2.649$ mm and $R_{56,2} = 17.50$ µm. The radiator has a period length of $\lambda_u = 19$ mm and is tuned to the output wavelength. The bunching along the electron bunch upstream from the radiator, the evolution of the FEL peak power along the radiator, as well as the spectrum and power profile at the same position in the radiator are presented in Figure 4. The bunching amplitude is approximately 9.5% and thus slightly smaller than the 11.2% predicted by

the simple analytical model (see Figure 2a), but still more than sufficient for an efficient amplification in the radiator.

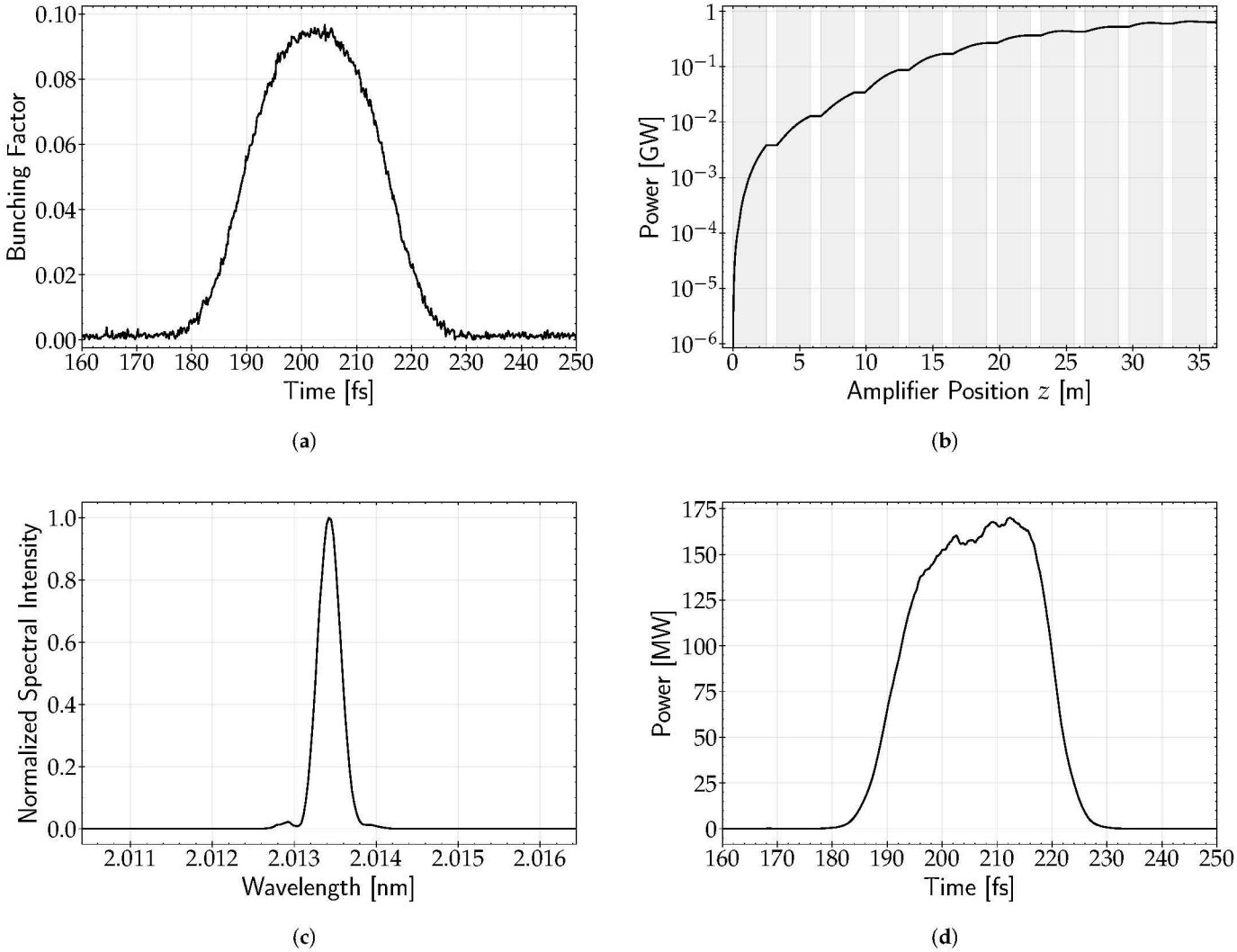

Figure 4. (**a**) Bunching along the electron bunch. (**b**) FEL peak power along the amplifier modules (gray). (**c**) Spectrum after the 5 modules of the amplifier. (**d**) Power profile after 5 modules of the amplifier.

2.2. Employing an Oscillator-Based Seeding Scheme in an Accelerator in Continuous-Wave or Burst-Mode Operation

A seeded oscillator-amplifier scheme is suitable for accelerators that can generate electron bunches at high repetition rates, as it requires a cavity length which matches the electron bunch repetition rate. The cavity roundtrip length should be $L_{cav} = c/(m \cdot f_{rep})$, where f_{rep} refers to the electron bunch separation and m is an integer which represents the number of roundtrips of the radiation before it meets again an electron bunch. For instance, when the electron bunches arrive with a frequency of 1 MHz, the total roundtrip cavity length should be $L_{cav} \approx 300$ m for $m = 1$. Alternatively, the radiation pulse can perform more than one roundtrip in between two consecutive bunches. However, in this case the total resonator reflectivity decreases with the number of passes m as R^m.

A superconducting accelerator can run in continuous wave (CW) or burst-mode operation. At FLASH [40,41], which operates in burst-mode, the bunch trains arrive with a repetition rate of 10 Hz with a flattop of 800 µs and a bunch spacing of 1 µs (1 MHz repetition rate). With a pulsed operation at 10 Hz as well, the flattop of the European XFEL is 600 µs with a 0.22 µs bunch separation (4.5 MHz) [42]. The exact number of bunches available depends on the operation mode and the sharing of those bunches among different

undulator beamlines. In the case of burst-mode operation, there is a specific number of bunches available to build-up the peak power and stability needed to deliver seeded FEL pulses. This is not an issue when the process starts with a low repetition rate seed laser source because the steady-state regime is reached within a few passes [22] as shown in Figure 5a, but it is critical when starting from shot noise, as we show in Figure 5b. The build-up regime is marked with a green background color. During this process, there must be positive net gain, and the peak power in each pass increases. The steady-state regime is marked with blue color in the same figure, and refers to the passes in the oscillator where the net gain is zero and the peak power per pass is constant. Comparing Figure 5a,b, there are more power fluctuations in the case where we start with a seed laser. This might be due to the fact that in this case we do not use a monochromator.

In burst-mode operation, the more bunches are used during the build-up process, the less bunches will be part of the steady-state regime when seeded radiation is generated. The steady-state can be maintained for a maximum number of passes defined by the difference between the available bunches in one bunch train and the number of bunches used during the build-up process. Taking as an example FLASH and the build-up regime shown in Figure 5b, we would need 18 bunches to take part in the build-up of the power, and the remaining 782 bunches would be part of the steady-state regime where the seeded radiation is generated.

A machine operated in CW mode offers a continuous number of bunches with a constant separation between them. For instance, SHINE in Shanghai will be operated in a CW mode and is expected to provide bunches with a continuous 1 MHz repetition rate [43]. The same repetition rate is planned for LCLS-II [44] as well. In this case, the build-up time needed becomes less important. It is possible to increase the number of passes in the build-up regime and ensure a smooth transition to the steady state. However, it becomes more important to verify how long the steady-state regime can be maintained before the process needs to be initiated again.

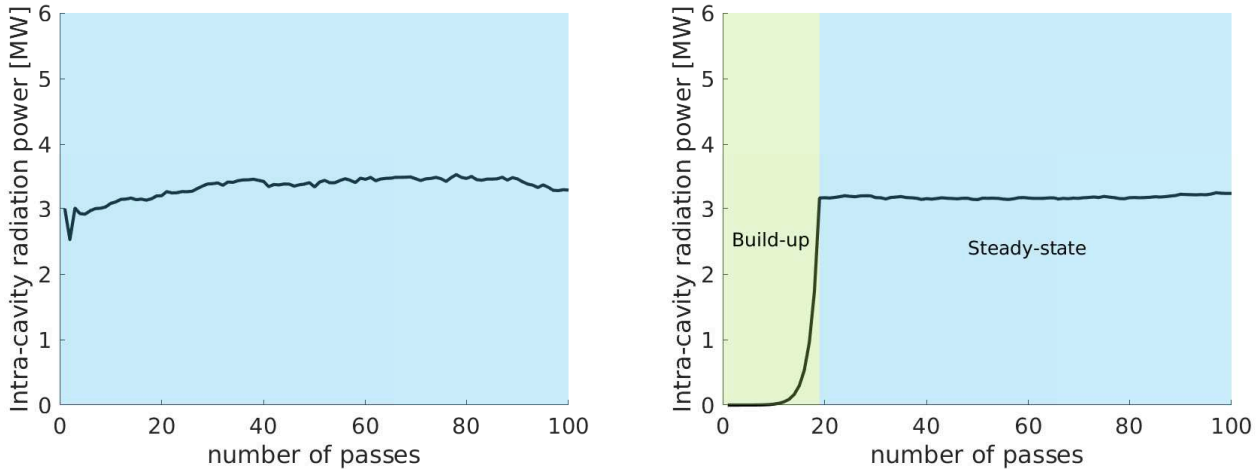

Figure 5. (**a**) Example of the peak power per pass in an oscillator starting with a low repetition rate seed laser. From the first pass already the net gain should be zero. In practice, it takes a few passes for the system to self-stabilize. (**b**) Example of the peak power per pass in an oscillator starting from shot-noise. For 19 passes the build-up regime where the net gain is positive is highlighted with a green color. At pass 19, the desired peak power level is reached and the steady state regime is entered, marked with a blue color. From this pass and onward, the net gain is reduced to zero and the peak power level is maintained in each pass.

3. Resonator Considerations

3.1. A Simple Model for the Reflectivity Requirements and Estimated Power Level in the Cavity

The transition between the build-up and the steady-state regime in the case of start-up from shot noise is discussed in more detail in Section 4, while here we focus on the steady-state operation of the modulator-amplifier. We maintain the generality of the discussion by using approximations to build a simple model that can be used to investigate the parameter space for the design requirements. In the steady-state regime, there is a number of conditions that need to be fulfilled:

- The input seed power needs to exceed the shot noise power of the electron beam by several orders of magnitude; otherwise, the SASE is not suppressed and the seeding process is not successful. Only a part of the seed power contributes to the exponential growth. Using for estimation the 1D cold FEL model this fraction amounts to 1/9. Assuming an excess of 3 orders of magnitude, the minimum input seed laser pulse peak power needs to be at least several 10 kW to 100 kW, depending on the exact electron beam parameters [45]. In addition, for seeding techniques it is required to induce an energy modulation of several times the initial energy spread which depends on the target harmonic to be amplified, the exact seeding scheme and the modulator length for given electron beam parameters. Typically, this requires a peak power that is larger than 100 kW.
- The saturation power downstream of the modulator needs to be well below the "natural" saturation to avoid large induced energy spread, which would suppress the amplification process at the amplifier. As a general rule, the energy spread downstream of the modulator σ_E relative to the electron beam energy E, should be considerably less than the FEL parameter of the amplifier ρ_{amp} [46], thus $\sigma_E/E \ll \rho_{amp}$ [45]. The maximum acceptable seed peak power after amplification in the modulator strongly depends on the length of the modulator with respect to the gain length, and thus on the power amplification and on the energy spread increase. For the sake of avoiding a specific parameter set, here we assume that saturation at the seed laser wavelength yields between 1 GW to several 10 GW. Assuming a margin of 3 orders of magnitude to avoid "heating" of the beam, the seed peak power after amplification needs to be limited to not more than several tens of MW.

The gain from shot noise to saturation of an FEL is around 9 orders of magnitude, which corresponds to about 20 power gain lengths (L_g). This means that there are 3 orders of magnitude between the minimum input peak power (P_{in}) and the maximum output peak power which are allowed to be lost in the cavity. Otherwise, either the minimum power is too close to shot noise or the maximum power too close to saturation. It is clear that these boundaries are not very strict and should only be seen as an approximation. It is known that the power along z develops as [46]:

$$P(z) = \frac{P_{in}}{9} \cdot e^{z/L_g}. \tag{1}$$

With a roundtrip reflectivity R, the power after a modulator length of L_{mod} should be $P(L_{mod}) = P_{in}/R$. This leads to

$$\frac{P_{in}}{R} = \frac{P_{in}}{9} \cdot e^{L_{mod}/L_g} \rightarrow L_{mod} = L_g \cdot \ln(\frac{9}{R}) \tag{2}$$

For the first approximately three power gain lengths we expect no FEL power amplification, and this is referred to as the lethargy regime. Assuming three orders of magnitude for the maximum allowed power amplification, the maximum modulator length is $9 \cdot L_g$ to compensate losses. The same equation can be used for design considerations; for instance, for a total reflectivity of 6%, the modulator should be roughly $5 \cdot L_g$. This result is indepen-

dent of the input seed laser power, however, in practice, the energy modulation process depends on both the input seed peak power and the length of the modulator as [47]:

$$\Delta E = \sqrt{\frac{P_{in}}{P_o}} \frac{m_e 2KL_{mod}\mathrm{JJ}}{\gamma w_0}, \tag{3}$$

where w_0 is the seed waist size, K is the dimensionless undulator parameter, m_e is the electron mass in keV, $P_0 \approx 8.7\,\mathrm{GW}$ [47], $\mathrm{JJ} = J_0(\xi) - J_1(\xi)$, where $\xi = K^2/(4+2K^2)$ and $J_{0,1}$ the Bessel function of the zeroth and first order. As the modulator is used both for energy modulation and amplification, both these aspects need to be taken into account for the exact design. Let us consider an example of these analytical estimations by means of a reasonable set of parameters: $\lambda_{seed} = 50\,\mathrm{nm}$, $K = 3.25$, $w_0 = 286\,\mu\mathrm{m}$, $\gamma = 2641.9$, $L_g = 1.12\,\mathrm{m}$. In Figure 6, we show the expected energy modulation for a combination of seed laser peak power and modulator length, calculated with Equation (3). In the same figure, we show the reflectivity required as expected by the 1D cold theory and Equation (1) with the dashed black vertical lines, as it is independent of the input seed laser power. It is clear that while the modulator length is fixed and is used to determine the amplification, for a given modulator length, it is still possible to use the seed laser peak power as a knob to adjust the energy modulation. In turn, the energy modulation is related to the energy spread which affects the FEL process in the amplifier, as already discussed. Note that while Equations (1) and (3) are well established approximations valid in the 1D case, diffraction effects should be also taken into account and the exact dependencies may deviate from this result.

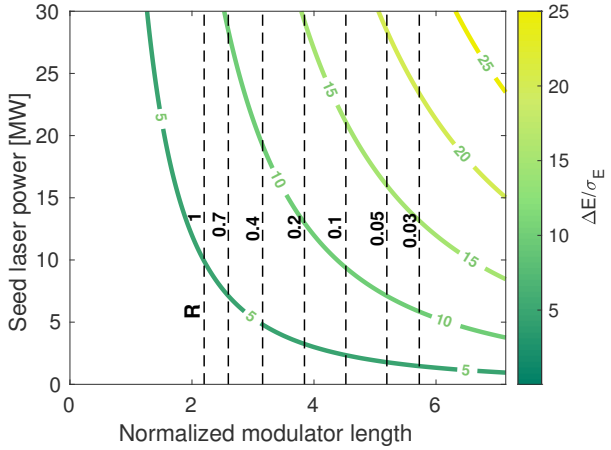

Figure 6. The color bar indicates the energy modulation achieved for combinations of seed laser peak powers (P_{in}) and modulator lengths (L_{mod}) and is calculated with Equation (3). The horizontal axis shows the normalized modulator length to the gain length (L_{mod}/L_g). The vertical dashed lines show the reflectivity R required for equilibrium between amplification and losses for different normalized modulator lengths, and is calculated with Equation (2).

3.2. Cavity Design Considerations

The numbers quoted so far are needed for the system to work, and should be complementary with a discussion on the technical feasibility of the resonator. The important questions here are if the downstream mirror, which will have the maximum power density, will be able to withstand it, and if mirrors with the required properties actually exist. We consider two operation regimes for the resonator: one at a wavelength between 200 nm and 300 nm, and one between 50 nm and 100 nm.

Regarding the reflectivity requirements, we expect that for wavelengths around 300 nm, the mirror choice will not pose an issue as there are options to choose from. Optics in this wavelength regime are used for current laser systems, such as dielectric

mirrors, with reflectivity and damage threshold that guarantee sustainable operation and have been studied for other storage ring FELs in the past as well [48]. The main challenge is faced for the working point in the XUV range between 100 nm and 50 nm, where no commonly used options are available. Here, we consider the upper limit in gain, where the roundtrip loss should not exceed a factor 1000 to avoid electron beam heating. Under normal incidence, this means that each mirror should reflect at least $1/\sqrt{1000} \approx 1/33$ or 3%. In case of a ring resonator with mirrors at 45 degree incidence angle, each should reflect more than $1/\sqrt{\sqrt{1000}} \approx 1/5.6$ or 18%. For example, we consider Molybdenum mirrors. At normal incidence, the reflectivity at 40 nm is ~6%, at 45 degree around 40% [49]. Both values exceed the requirements. Note that a gain of 1000 is an upper limit that would require a relatively long modulator. However, it is preferred to operate at a lower gain if the reflectivity of mirrors allows it.

Here, we consider simple estimations in order to calculate the power density for a Gaussian beam. Assuming a Gaussian beam with a waist at the end of the undulator, the size of the spot at the mirror is [47]:

$$w^2(L) = w_0^2\left(1 + \left(\frac{L}{\ell}\right)^2\right), \tag{4}$$

where L is the distance from the undulator to the mirror, w_0 is the spotsize at the waist and ℓ is the Rayleigh length. With the distance to the mirror much larger than the Rayleigh length and remembering that for a Gaussian beam $\pi w_0^2 = \lambda\ell$ with λ the radiation wavelength, the dependence of the beam radius on the distance becomes nearly linear and we can rewrite Equation (4) as

$$w^2(L) \approx \left(\frac{L\lambda}{\pi w_0}\right)^2 \approx \left(\frac{L\lambda}{\pi\sigma_b}\right)^2, \tag{5}$$

where we have approximated the spotsize of the radiation with the electron beam size σ_b. Since the mirror has an angle with respect to the radiation in one plane only, the area of the radiation on the mirror for a transversely symmetric beam can be approximated as:

$$S \approx \left(\frac{L\lambda}{\pi\sigma_b}\right)^2 \frac{1}{\sin\alpha}, \tag{6}$$

with α the glancing angle.

Assuming that the fraction of the pulse energy that is not reflected by the mirror is in fact absorbed, the power density P_d absorbed is

$$P_d = \frac{E_p}{S} \cdot (1 - R) = E_p(1 - R)\sin\alpha\left(\frac{\pi\sigma_b}{L\lambda}\right)^2, \tag{7}$$

with E_p the pulse energy.

Here, we take the example of FLASH2 and the existing mirrors commonly used in FLASH operation to demonstrate a feasible working point. For a wavelength of 15 nm with a mirror 15 m downstream of the undulator under a glancing angle of 1 degree, from Equation (6) the spot size is approximately 0.3 cm^2, assuming a 100 µm beam size. With a reflectivity of 99% ($R = 0.99$) and 1 mJ of pulse energy per second for a single pulse, the power density is around 1 mW/0.3 cm^2, or up to 17 W/cm^2 for a pulse train of 5000 pulses per second. Under these assumptions and taking into account the reflectivity, the absorbed power of FLASH2 on the mirror is up to 170 mW/cm^2 for 15 nm.

For a modulator with the mirror at normal incidence at the same distance of 15 m, the same electron beam size and a wavelength of 50 nm, the spot is from Equation (5) approximately 2.4 by 2.4 mm. Assuming again Molybdenum mirrors with 95% absorption, the pulse energy should not exceed 2 µJ in order to avoid an absorbed power density higher than 170 mW/cm^2. At 45 degrees with 60% absorption, the pulse energy would be approximately 5 µJ. Assuming a typical pulse duration of 100 fs, the peak power is

therefore 20 MW (or 50 MW for the 45 degree mirror case), which is consistent with the values mentioned earlier for FLASH. For a CW-FEL, the numbers are more critical because of the larger number of bunches per second.

Finally, we would like to comment on the geometry of the optical feedback system. There is a number of components needed in order to maintain a stable operation and diagnose the radiation field properties. The intensity of the seed laser, which in this case is the intensity inside the resonator, needs to be regulated and therefore measured for a large wavelength range without significant distortion of the radiation field. Furthermore, with the system starting from noise, the noise needs to be suppressed, which is best done with a grating. Finally, the radiation needs to be refocused in the middle of the modulator. Therefore, the actual resonator will have a more complicated geometry than depicted earlier. A ring resonator could include all needed elements, but other geometries should be considered and compared depending on the wavelength requirements and space constraints of a specific facility. The technical design and specifications are, however, beyond the scope of this paper.

4. Simulation Results and Implementation Considerations for Oscillator-Based Seeding Starting from Shot Noise

In this section, we focus on an HGHG-based oscillator scheme as shown in Figure 1 and more specifically, in the case of an oscillator-FEL starting from shot noise. As shown in Figure 5b, when the process in the cavity starts from shot noise, there are two separate operation regimes to be considered. For a transition from positive net gain ("build-up") to zero net gain ("steady-state"), the gain has to be reduced. Here, we discuss different methods that could be applied in order to achieve control over the power gain in the resonator. In all cases we use the same set of simulation parameters, which is summarized in Table 1, and the modulator is resonant with 50 nm wavelength. For the sake of simplicity, here we restrict ourselves to the case of a relative energy modulation $A = \Delta E/\sigma_E = 7$, meaning that the amplitude of the energy modulation ΔE after the modulator is seven times larger than the initial energy spread σ_E in the steady-state regime. As seen in Equation (3), for given lattice, electron beam parameters and constant waist size, the energy modulation is stabilized if the input peak power in the modulator P_{in} is stable too. All simulations here are done with Genesis 1.3 for the FEL process [39], while the radiation field in the cavity is treated with ocelot [50], which accounts for the slippage, reflectivity, focusing, and monochromatization.

Table 1. Electron beam parameters used in simulations.

Electron Beam Parameters	
Energy	1350 MeV
Energy spread	120 keV
Peak current	1 kA (flat-top)
Pulse duration	300 fs
Normalized Emittance	1 mm · mrad

4.1. Reflectivity Adjustment

The most direct way to control the net gain is to adjust the resonator reflectivity. In this case, initially the reflectivity ($R_{build-up}$) is as high as possible to enable a fast build-up of the power and then, when the desired peak power level is reached, the reflectivity has to drop to the value R_{equil}, which ensures equilibrium between losses and power gain. The reflectivity applied during the build-up process, $R_{build-up}$, is determined by the maximum total reflectivity allowed by the mirrors, and the maximum change in reflectivity that can be supported by a filter within the time separation of two consecutive bunches. The larger the difference in reflectivity $\Delta R = R_{build-up} - R_{equil}$ is, the higher the net gain and the faster the steady-state regime will start, as shown in Figure 7a. For the present setup of resonator and beam parameters shown in at Table 1, the reflectivity at equilibrium is $R_{equil} = 10.6\%$,

including the losses in the monochromator. With $R_{build-up} = 14\%$, 46 passes are required in the build-up regime in order to reach a relative energy modulation of $A = 7$, while a reflectivity of $R_{build-up} = 12\%$ requires 99 passes. It is also possible to apply the reflectivity change in steps if a fast change is not possible. For instance, for the reflectivity change required as shown in Figure 7b, it is possible to apply the $\Delta R = 3.4\%$ (from $R_{build-up} = 14\%$ to $R_{equil} = 10.6\%$) in steps of $\Delta R = 0.34\%$ in 10 passes. In the case of a burst-mode of operation, the number of steps must be reasonably small compared to the number of bunches at the steady-state. In the case of a continuous wave operation, these steps can be as small as required by the hardware limitations.

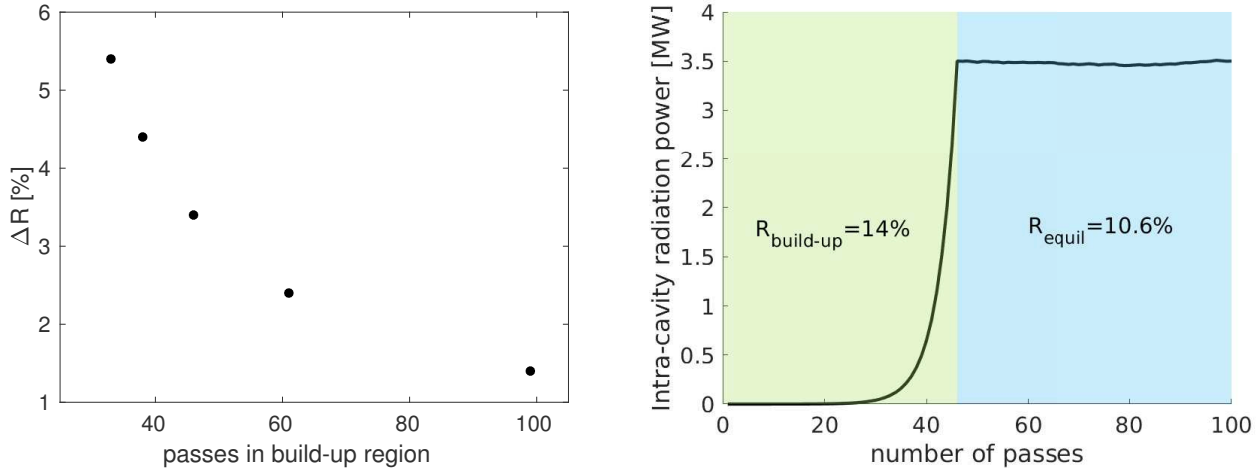

(**a**) (**b**)

Figure 7. (**a**) In this plot, the number of passes needed to reach steady-state as function of reflectivity change, $\Delta R = R_{build-up} - R_{equil}$, is shown. We assume that the build-up process is over when the energy modulation is at least A = 7. (**b**) Example of $\Delta R = 3.4\%$. For the first 46 passes the reflectivity is set to $R_{build-up} = 14\%$ and from the 47th pass onward the reflectivity drops to $R_{equil} = 10.6\%$ and the net gain is zero. As a result, the peak power is stabilized.

In practice, the reflectivity change can be implemented by adding a filter in the return path of the radiation field. A total reflectivity change of several percent is currently not possible to be applied within 1 µs, but would be possible in several steps during a transition time. For this reason, this method would be an option in CW machines, as it is currently unlikely to function in burst-mode in view of time constraints.

4.2. Longitudinal Overlap between Electron Bunch and the Recirculating Light Pulses

Another method to obtain gain control is by affecting the longitudinal overlap between the electron bunch and the stored radiation field. A change in cavity length would change the arrival time of the radiation pulse, a procedure known as cavity detuning. The exact amount of the detuning or delay needed to transition between positive net gain and zero net gain depends on the electron bunch length. Here, we have assumed a 300 fs flat-top current distribution for the electron bunch as an example study.

For all passes, the reflectivity is set to a value R_{set} which is larger than R_{equil}, namely, the reflectivity, which leads to zero net gain when the longitudinal synchronism between the electron bunches and the recirculated seed pulse is optimum. Here, we define the cavity length L_{cav} for which the detuning is zero ($\Delta L_{cav} = 0$), as the cavity length for perfect synchronism between the radiation pulses and consecutive electron bunches for no slippage, thus it is the cold cavity length. Due to slippage effects, perfect synchronism is achieved for longer cavity lengths ($\Delta L_{cav} > 0$) that allow the longitudinally advanced radiation pulse to be delayed. As in this case we assume that the reflectivity cannot be reduced, we keep the reflectivity constant over all passes and we de-tune the cavity by ΔL_{cav} to reduce the net gain in the steady-state regime. The detuning and the reflectivity

are two complementary knobs. The larger the reflectivity difference $\Delta R = R_{set} - R_{equil}$ is, the longer the detuning is needed.

In Figure 8a, a cavity detuning is simulated for a range of set reflectivities R_{set} between 11% and 15% . The cavity detuning curve for each reflectivity shows how much the length of the cavity should be shifted to move from the maximum net gain (shown with the vertical arrow), to zero net gain (intersections between the horizontal dashed line and detuning curve). The cavity detuning for maximum power gain is independent of the total reflectivity as expected, as it depends on the total slippage per pass, which is in turn dependent on the wavelength, the periods of the modulator and the group velocity of the field. Taking again the example of $R_{set} = 14\%$, in Figure 7a we need 46 passes to reach the desired in-cavity peak power level with the optimum detuning of $\Delta L_{cav} = 2.7\,\mu$m, and from Figure 8b we see that a detuning of $\Delta L_{cav} = -14.1\,\mu$m keeps the in-cavity peak power level constant. The result is shown in Figure 8b, where the cavity length is shifted by 16.8 µm and equilibrium is reached and maintained.

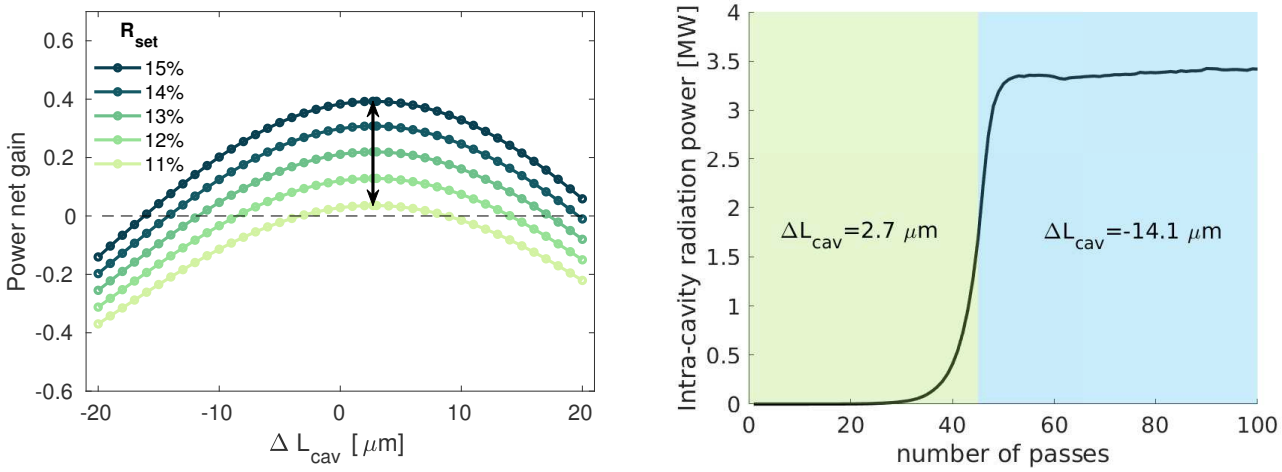

(**a**) (**b**)

Figure 8. (**a**) Detuning curves for a 300 fs flat-top electron beam. The optimum detuning length is at $\Delta\lambda = 2.7\,\mu$m, for all set reflectivities, as shown with the vertical arrow. The zero net gain point shown with the horizontal dashed line, shows the detuning that needs to be applied to reach equilibrium for each total reflectivity R_{set}. Keeping the reflectivity constant and changing the cavity length can transition the system from positive to zero net gain. We remind the readers that the power net gain has no units as it is the difference between the peak power at the beginning of pass n + 1 and at pass n, divided by the peak power at pass n. (**b**) With an oscillator starting from the random fluctuation of the electron beam distribution, a transition between amplification of the power and maintenance of the peak power is achieved by detuning the cavity length from $\Delta L_{cav} = 2.7\,\mu$m to $\Delta L_{cav} = -14.1\,\mu$m. For all passes the reflectivity is $R_{set} = 14\%$.

For the implementation of this technique there are different options that can be considered. When detuning the cavity length, the position of one or more mirrors needs to be adjusted within µm and with a MHz repetition rate. This depends heavily on the mirror choice and mirror size and weight. As an alternative solution, in the past a similar dynamic cavity desynchronization was considered for FELIX [51] in order to control the growth rate and the final power at saturation and the fluctuations in power [52,53]. It was proposed that instead of mechanically adjusting the mirrors, it is preferable to ramp the electron bunch repetition rate frequency by Δf_{rep} to achieve a cavity detuning of $\Delta L_{cav} = L\Delta f_{rep}/f_{rep}$ [53]. In this case, a dynamic desynchronization along the bunch train is important.

As a final remark, it is important to point out that the cavity detuning results in a change in the temporal and spectral distribution of the stored FEL pulse. This has been extensively discussed in FEL oscillators in the past [54–56]. The consequences on the properties of the output FEL should be carefully considered before applying this method for power gain control.

4.3. Optical Klystron

Another well-established method of gain control in FELs is the use of an Optical Klystron (OK), first introduced in [57]. It was originally introduced for gain control in oscillator FELs [58], but its application has been expanded. It has been used as a method to speed up the FEL process in SASE operation, when the total amplifier length is not sufficient for a given wavelength [59–61]. In addition, it is used in a seeding scheme when the seed laser peak power is not sufficient to increase the energy modulation required in seeding [17]. The simplest configuration of an optical klystron consists of two undulators tuned at the same resonant wavelength and a dispersive section in between them. The electron beam travels in the first undulator starting from some initial conditions (noise, or external seed) and a relatively weak energy modulation is induced. Then, the dispersive element modifies the electron beam phase space. This way, the bunching at this fundamental wavelength is increased, and the bunched electron beam generates coherent emission in the second undulator with increased gain. The dependence of the power gain on the longitudinal dispersion is a useful knob for our setup.

In an oscillator, the two modulator sections separated by the dispersive section are in the resonator as shown in Figure 9. A 1D theory of optical klystron is discussed in [61] and a recent revision can be found in [62]. The optimum longitudinal dispersion depends on the energy spread and in our case can be estimated as

$$R_{56,1} = \frac{\lambda_{res}}{2\pi\delta} \,, \tag{8}$$

where δ is the relative energy spread. With the studied parameter space, the optimum longitudinal dispersion is predicted as $R_{56,1}$ = 89 µm. Note that the sum of the length of modulator 1 and modulator 2 in Figure 9 is equal to the length of the modulator in Figure 1, so the power gain increase is introduced by chicane 1 only, and not by increasing the length of the modulator.

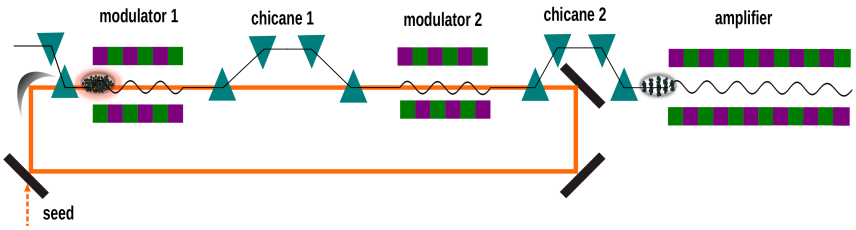

Figure 9. In an oscillator-based HGHG scheme, an optical klystron can be employed. To do so, the cavity contains two modulators separated by a chicane. This way this chicane can be tuned to control the gain per pass.

In order to transition to the zero net gain regime, the $R_{56,1}$ should initially be set to a value close to the optimal, and later on tuned to another value which would reduce the gain in the second modulator. In Figure 10a, we show the net gain achieved for different reflectivities and $R_{56,1}$. The $R_{56,1}$ at the steady state is determined by the intersection of the curves and the horizontal dashed line, which shows the zero net gain. We are interested in the range $R_{56,1} < 75$ µm, because a too large $R_{56,1}$ would cause an over-rotation of the longitudinal phase space which is not useful, as we still need to increase the bunching at a harmonic of the seed wavelength with the $R_{56,2}$. The optimum longitudinal dispersion appears at around $R_{56,1} = 73$ µm, which is approximately in agreement with Equation (8). Note, here, that the reflectivities required with the optical klystron are dramatically reduced, by more than an order of magnitude, when we compare to Figure 8a. As an example, with a reflectivity $R_{set} = 0.38\%$, we can build-up the peak power needed for seeding with $R_{56,1} = 42.5$ µm, and after 19 passes change the longitudinal dispersion of the first chicane to $R_{56,1} = 30$ µm to achieve zero net gain, and stable peak power of the radiation field per

pass as shown in Figure 10b. Note, here, that the input peak power is considerably lower in the order of 120 kW compared to the roughly 3.5 MW needed in all other gain-control methods presented already, to achieve the same energy modulation $A = 7$. In addition, the reflectivity required, $R_{set} = 0.38\%$, which considerably relaxes the requirements on the mirror specifications.

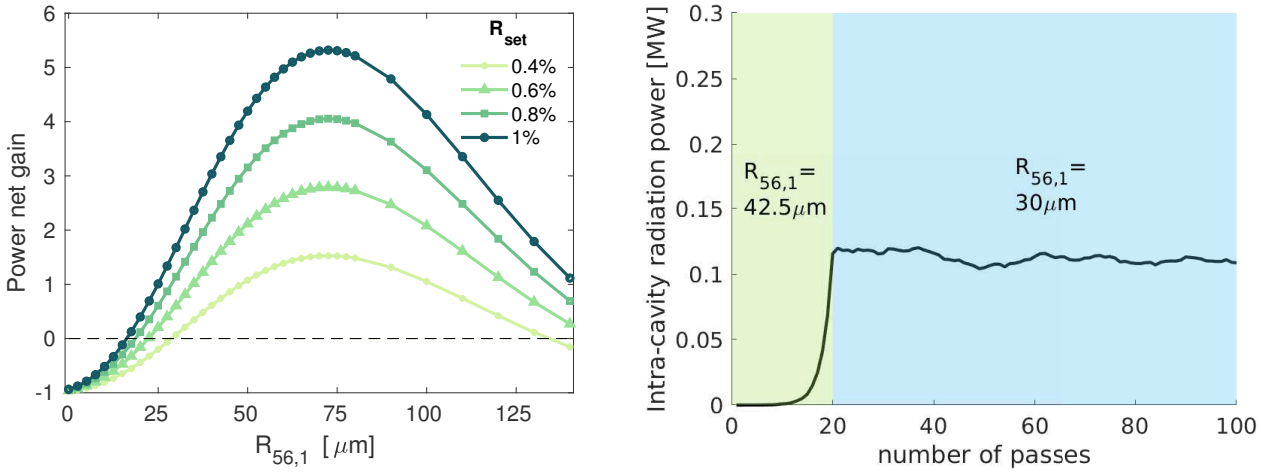

(**a**) (**b**)

Figure 10. (**a**) Changing the $R_{56,1}$ of the chicane affects drastically the gain in power. Here we show the net power gain for selected set reflectivities R_{set}, between 0.4% and 1%. The horizontal line shows the zero net gain. (**b**) With a reflectivity $R_{set} = 0.38\%$, it is possible to transition from positive gain to zero gain by adjusting the longitudinal dispersion of chicane1 as shown in Figure 8, from $R_{56,1} = 42.5$ µm to $R_{56,1} = 30$ µm, respectively.

The optical klystron has many advantages. As already explained, the first one is that it makes the transition from positive to zero net gain possible. In addition, it increases the gain both in the positive gain regime and in the zero net gain regime as $R_{56,1} \neq 0$ as well. This relaxes significantly the requirements in mirror reflectivity in the XUV range. Moreover, the optical klystron could be used as an active tuning tool to adjust the gain per pass and absorb different sources of jitter which contribute to gain changes. Concerning technical requirements, a chicane consisting of fast kickers for this purpose should be able to change the R_{56} by several µm and with a MHz repetition rate. Stripline fast kickers are already standard technology and are, for instance, used at the European XFEL for extracting individual electron bunches with up to 4.5 MHz repetition rate [63,64]. Let us assume that a change of 10 µm is sufficient to transition from positive net gain to zero net gain. The longitudinal dispersion of the chicane is approximately $R_{56} \approx L\theta^2$, where L is the distance between the first and second dipole of a chicane and θ is the bending angle of the first dipole. A kicker adds an angle

$$\Delta\theta[\mu\text{rad}] = L_{kicker}[\text{cm}]B_{kicker}[\text{Gauss}]/E_b[\text{GeV}],$$

with L_{kicker} and B_{kicker} being the length and field of the kicker and E_b the electron beam energy. With these kickers, a kick angle of 0.6 mrad can be achieved with $E_b = 1$ GeV and the change of R_{56} shown in Figure 10b would be possible within 1 µs. It is important to ensure that implementing this change in R_{56} will not affect the stability of the system. Using the kickers only in the build-up regime would ensure stability during the steady-state regime. For the build-up regime, the stability is not so important, as long as the peak power is reached, since during these passes no seeded radiation is generated.

5. Comparison of Simulation Results

Until now, we have only discussed about the process in the modulator and resonator. In this section, we compare simulation results at a final wavelength of 4.167 nm, reached with different schemes and this time we show the final FEL pulses generated at the amplifier. For the HGHG simulations, this wavelength is the 12th harmonic of a 50 nm resonant modulator. We consider the following four cases:

- A SASE setup, starting from shot noise and without changing any electron beam parameters. The FEL pulse is extracted at the same position as the seeding simulations.
- A single-pass standard HGHG setup, starting with an ideal Gaussian seed laser pulse instead.
- An HGHG seeded oscillator-amplifier starting with a low repetition rate seed laser. This scheme was discussed in detail in [22]. For the first electron bunch an external seed laser pulse is injected, and then the seed pulse is stored in the cavity.
- An HGHG seeded oscillator-amplifier system starting from shot noise. This was described in detail in Section 4. A reflectivity change from $R_{build-up} = 14\%$ to $R_{equil} = 10.6\%$ was used to transition from positive to zero net gain.

In Table 2, we have summarized the main simulation results for the four different cases, and in Figure 11 we show the final spectra for the four different cases with the same final wavelength of 4.167 nm. In addition, for completeness, we have added the pulse properties of the output FEL at 2 nm with the EEHG simulations discussed in Section 2.1.2. The output FEL is shown in Figure 4. Note that the peak power is comparable for all HGHG seeded pulses as expected; however, as the resulting pulse duration differs, the bandwidth cannot be directly compared. It is important to emphasize that a single-spike spectrum was generated in all seeded schemes. The power spectral density in the multi-pass HGHG starting with a seed laser, and in the standard single-pass HGHG are almost identical, while the multi-pass HGHG starting from shot noise seems to have almost an order of magnitude higher spectral density as shown in Figure 11d. In this case, we have used a monochromator with an rms bandwidth of $\Delta\lambda/\lambda = 2.5 \times 10^{-4}$ in the resonator, which stretches the radiation pulses and filters the radiation in the frequency domain. Because of this, the result in Figure 11d deviates compared to the other two HGHG cases.

Table 2. Simulation results for final FEL pulse at the same position along amplifier. For the multi-pass simulations, we examine the FEL pulse after 100 passes. For the SASE, we calculate based on the average over 50 simulations with different shot noise. For EEHG, we consider the simulation results of a 2 nm output FEL shown in Figure 4.

	Peak Power	$\Delta\lambda_{FWHM}/\lambda$	**rms Pulse Duration**
SASE	3 MW	2×10^{-3}	75 fs
Standard HGHG	1.2 GW	1.6×10^{-4}	20 fs
multi-pass HGHG (seed)	1.2 GW	2×10^{-4}	27 fs
multi-pass HGHG (shot-noise)	1.1 GW	5×10^{-5}	60.6 fs
single-pass EEHG	0.18 GW	1.6×10^{-4}	11.35 fs

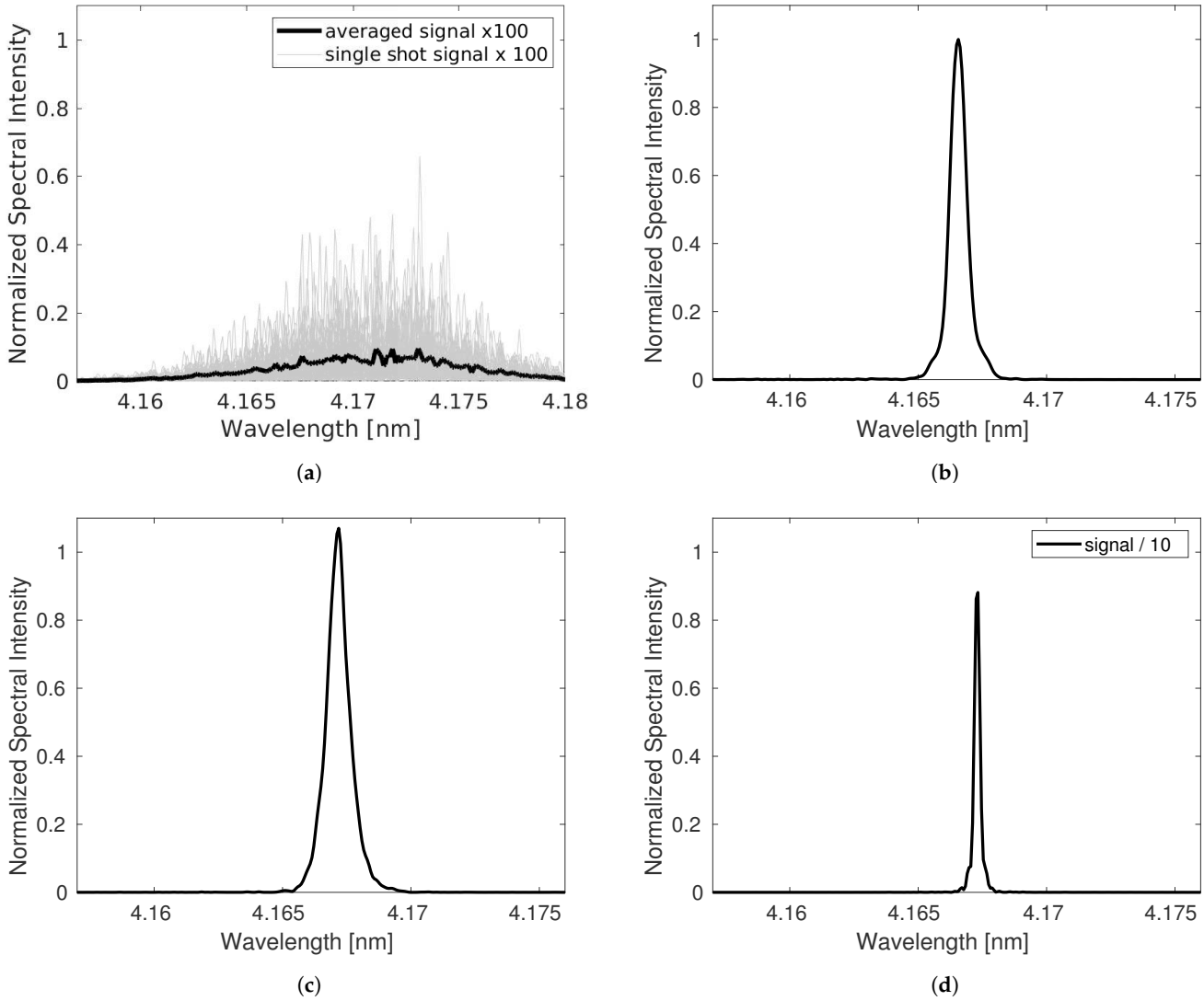

Figure 11. Spectra of final FEL pulse at the same position at the amplifier and with the same electron beam parameters shown at Table 1. The spectral intensity is normalized to the peak intensity calculated at the standard single-pass HGHG simulation. (**a**) SASE. Please notice the extended horizontal axis. The average SASE spectrum over 50 shots is shown with the black line. (**b**) Standard HGHG in a single-pass. (**c**) Oscillator-FEL starting with an external seed laser pulse. (**d**) Oscillator-FEL starting from shot-noise.

6. Discussion

In this paper, we described different seeding schemes that can benefit by employing an oscillator setup to increase the repetition rate of a seeded FEL. We presented an overview of simulations and requirements for its implementation. We developed a simple model to estimate the amplification and modulation process in the modulator. This gave an insight into the design of the resonator in terms of modulator length, resonator requirements, and feasibility of the implementation of this scheme. Then, we focused on simulation results of an HGHG scheme. We showed that there is a number of methods that could be used to dynamically control the power gain in the resonator when the process starts from shot-noise and we compared the performance of a single pass HGHG, a multi-pass HGHG starting with a low repetition rate seed laser and of SASE, which is to be considered as our background.

Where so far the wavelength range mentioned here could only be reached with an EEHG scheme, the use of a resonator now would make it possible to reach the same wavelength with an HGHG scheme. Alternatively, starting with a shorter wavelength in

an EEHG scheme, the use of the resonator could push the minimum wavelength beyond the water window and transition metals, making seeding in this important wavelength range possible. These options will be studied in future studies.

In addition, there are still a number of considerations that need to be addressed as we are moving towards more detailed studies for the realization of this scheme. Even though first stability studies were presented in [22], it is still crucial to study the stability of this scheme over several passes with a non-ideal electron beam, including imperfections and energy chirp effects. In addition, there are other important questions related to its implementation, such as how the repetition rate can be adjusted when experiments need a lower repetition rate, the space constraints to insert mirrors when the longitudinal dispersion required for seeding at short wavelengths is small, the requirements in terms of diagnostics for the recirculating radiation field, and realizing wavelength tunability. These are expected to be addressed in future work.

Author Contributions: Conceptualization, B.F.; data curation, G.P. and F.P.; validation, G.P., B.F. and G.G.; formal analysis, G.P.; writing—Original draft preparation, G.P.; writing—Review and editing, G.P., S.A., B.F., G.G., T.L., F.P., L.S. and J.Z.; project administration, G.P. and G.G. All authors have read and agreed to the published version of the manuscript.

Funding: This work was supported by the Impuls- und Vernetzungsfond der Helmholtz-Gemeinschaft e.V. within the CAS-Helmholtz International Laboratory on Free-Electron Laser Science and Technology (CHILFEL), grant number InterLabs-0002.

Institutional Review Board Statement: Not applicable.

Informed Consent Statement: Not applicable.

Data Availability Statement: Not applicable.

Acknowledgments: The authors would like to thank Fred Bijkerk for consultation regarding mirrors in the EUV, Frank Obier for information on kickers, Enrico Allaria and Pardis Niknejadi for useful discussions, and the Maxwell computational resources operated at Deutsches Elektronen-Synchrotron (DESY), Hamburg, Germany. Finally the authors thank Chao Feng, and Elke Ploenjes-Palm for a careful proofreading of the manuscript.

Conflicts of Interest: The authors declare no conflict of interest.

References

1. Saldin, E.L.; Schneidmiller, E.A.; Yurkov, M.V. *The Physics of Free Electron Lasers*; Springer: Berlin/Heidelberg, Germany, 2000.
2. Saldin, E.; Schneidmiller, E.; Yurkov, M. Statistical Properties of Radiation from VUV and X-ray Free Electron Laser. *Opt. Commun.* **1998**, *148*, 383–403. [CrossRef]
3. Amann, J.; Berg, W.; Blank, V.; Decker, F.J.; Ding, Y.; Emma, P.; Feng, Y.; Frisch, J.; Fritz, D.; Hastings, J.; et al. Demonstration of self-seeding in a hard-X-ray free-electron laser. *Nat. Photonics* **2012**, *6*, 693–698. [CrossRef]
4. Geloni, G.; Kocharyan, V.; Saldin, E. A novel self-seeding scheme for hard X-ray FELs. *J. Mod. Opt.* **2011**, *58*, 1391–1403. [CrossRef]
5. Rosenzweig, J.; Alesini, D.; Andonian, G.; Boscolo, M.; Dunning, M.; Faillace, L.; Ferrario, M.; Fukusawa, A.; Giannessi, L.; Hemsing, E.; et al. Generation of ultra-short, high brightness electron beams for single-spike SASE FEL operation. *Nucl. Instrum. Methods Phys. Res. Sect. Accel. Spectrometers Detect. Assoc. Equip.* **2008**, *593*, 39–44. [CrossRef]
6. Marinelli, A.; MacArthur, J.; Emma, P.; Guetg, M.; Field, C.; Kharakh, D.; Lutman, A.; Ding, Y.; Huang, Z. Experimental demonstration of a single-spike hard-X-ray free-electron laser starting from noise. *Appl. Phys. Lett.* **2017**, *111*, 151101. [CrossRef]
7. Prince, K.; Allaria, E.; Callegari, C.; Cucini, R.; Giovanni, D.N.; Di Mitri, S.; Diviacco, B.; Ferrari, E.; Finetti, P.; Gauthier, D.; et al. Coherent control with a short-wavelength Free Electron Laser. *Nat. Photonics* **2016**, *10*, 176–179. [CrossRef]
8. Gauthier, D.; Ribič, P.R.; De Ninno, G.; Allaria, E.; Cinquegrana, P.; Danailov, M.B.; Demidovich, A.; Ferrari, E.; Giannessi, L. Generation of Phase-Locked Pulses from a Seeded Free-Electron Laser. *Phys. Rev. Lett.* **2016**, *116*, 024801. [CrossRef] [PubMed]
9. Gauthier, D.; Allaria, E.; Coreno, M.; Cudin, I.; Dacasa, H.; Danailov, M.; Demidovich, A.; Di Mitri, S.; Diviacco, B.; Ferrari, E.; et al. Chirped pulse amplification in an extreme-ultraviolet free-electron laser. *Nat. Commun.* **2016**, *7*, 13688. [CrossRef] [PubMed]
10. Gorobtsov, O.; Mercurio, G.; Capotondi, F.; Skopintsev, P.; Lazarev, S.; Zaluzhnyy, I.; Danailov, M.; Dell'Angela, M.; Manfredda, M.; Pedersoli, E.; et al. Seeded X-ray free-electron laser generating radiation with laser statistical properties. *Nat. Commun.* **2018**, *9*, 4498. [CrossRef]
11. Yu, L.H.; Babzien, M.; Ben-Zvi, I.; DiMauro, L.F.; Doyuran, A.; Graves, W.; Johnson, E.; Krinsky, S.; Malone, R.; Pogorelsky, I.; et al. High-Gain Harmonic-Generation Free-Electron Laser. *Science* **2000**, *289*, 932–934. [CrossRef]

12. Allaria, E.; Cinquegrana, P.; Cleva, S.; Cocco, D.; Cornacchia, M.; Craievich, P.; Cudin, I.; D'Auria, G.; Dal Forno, M.; Danailov, M.; et al. Highly coherent and stable pulses from the FERMI seeded free-electron laser in the extreme ultraviolet. *Nat. Photonics* **2012**, *6*, 699–704. [CrossRef]
13. Xiang, D.; Stupakov, G. Echo-enabled harmonic generation free electron laser. *Phys. Rev. ST Accel. Beams* **2009**, *12*, 030702. [CrossRef]
14. Feng, C.; Deng, H.; Zhang, M.; Wang, X.; Chen, S.; Liu, T.; Zhou, K.; Gu, D.; Wang, Z.; Jiang, Z.; et al. Coherent extreme ultraviolet free-electron laser with echo-enabled harmonic generation. *Phys. Rev. Accel. Beams* **2019**, *22*, 050703. [CrossRef]
15. Ribič, P.; Abrami, A.; Badano, L.; Bossi, M.; Braun, H.H.; Bruchon, N.; Capotondi, F.; Castronovo, D.; Cautero, M.; Cinquegrana, P.; et al. Coherent soft X-ray pulses from an echo-enabled harmonic generation free-electron laser. *Nat. Photonics* **2019**, *13*, 1–7. [CrossRef]
16. Lechner, C.; Ackermann, S.; Azima, A.; Aßmann, R.; Biss, H.; Drescher, M.; Faatz, B.; Grattoni, V.; Hartl, I.; Hartwell, S.; et al. Seeding R&D at sFLASH. In Proceedings of the FEL'19, Geneva, Switzerland, 26–30 August 2019; Number 39 in Free Electron Laser Conference; pp. 230–233. [CrossRef]
17. Yan, J.; Gao, Z.; Qi, Z.; Zhang, K.; Zhou, K.; Liu, T.; Chen, S.; Feng, C.; Li, C.; Feng, L.; et al. Self-Amplification of Coherent Energy Modulation in Seeded Free-Electron Lasers. *Phys. Rev. Lett.* **2021**, *126*, 084801. [CrossRef] [PubMed]
18. Wang, X.; Feng, C.; Faatz, B.; Zhang, W.; Zhao, Z. Direct-Amplification Enabled Harmonic Generation for Seeding a High-Repetition-Rate Free-Electron Laser. 2021. Available online: http://xxx.lanl.gov/abs/2103.11971 (accessed on 10 May 2021).
19. Ackermann, S.; Faatz, B.; Grattoni, V.; Lechner, C.; Paraskaki, G.; Geloni, G.; Serkez, S.; Tanikawa, T.; Hillert, W. High-Repetition-Rate Seeding Schemes Using a Resonator-Amplifier Setup. In Proceedings of the International Free Electron Laser Conference (FEL'19), Hamburg, Germany, 26–30 August 2019; Number 39 in International Free Electron Laser Conference; JACoW: Geneva, Switzerland, 2019; [CrossRef]
20. Paraskaki, G.; Ackermann, S.; Faatz, B.; Grattoni, V.; Lechner, C.; Mehrjoo, M.; Geloni, G.; Serkez, S.; Tanikawa, T.; Hillert, W. Study of a Seeded Oscillator-Amplifier FEL. In Proceedings of the International Free Electron Laser Conference (FEL'19), Hamburg, Germany, 26–30 August 2019; Number 39 in International Free Electron Laser Conference; JACoW: Geneva, Switzerland, 2019; [CrossRef]
21. Ackermann, S.; Faatz, B.; Grattoni, V.; Kazemi, M.M.; Lang, T.; Lechner, C.; Paraskaki, G.; Zemella, J.; Geloni, G.; Serkez, S.; et al. Novel method for the generation of stable radiation from free-electron lasers at high repetition rates. *Phys. Rev. Accel. Beams* **2020**, *23*, 071302. [CrossRef]
22. Paraskaki, G.; Grattoni, V.; Lang, T.; Zemella, J.; Faatz, B.; Hillert, W. Optimization and stability of a high-gain harmonic generation seeded oscillator amplifier. *Phys. Rev. Accel. Beams* **2021**, *24*, 034801. [CrossRef]
23. Dattoli, G.; Giannessi, L.; Ottaviani, P.; Torre, A. Dynamical behavior of a free-electron laser operating with a prebunched electron beam. *Phys. Rev. E Stat. Phys. Plasmas Fluids Relat. Interdiscip. Top.* **1994**, *49*, 5668–5678. [CrossRef]
24. Dattoli, G.; Faatz, B.; Giannessi, L.; Ottaviani, P.L. The tandem FEL dynamic behavior. *IEEE J. Quantum Electron.* **1995**, *31*, 1584–1590. [CrossRef]
25. Dattoli, G.; Giannessi, L.; Ottaviani, P. Oscillator-amplifier free electron laser devices with stable output power. *J. Appl. Phys.* **2004**, *95*, 3211. [CrossRef]
26. Kim, K.J.; Shvyd'ko, Y.; Reiche, S. A Proposal for an X-Ray Free-Electron Laser Oscillator with an Energy-Recovery Linac. *Phys. Rev. Lett.* **2008**, *100*, 244802. [CrossRef]
27. Nguyen, D.C.; Sheffield, R.L.; Fortgang, C.M.; Goldstein, J.C.; Kinross-Wright, J.M.; Ebrahim, N.A. First lasing of the regenerative amplifier FEL. *Nucl. Instrum. Methods Phys. Res. A* **1999**, *429*, 125–130. [CrossRef]
28. Faatz, B.; Feldhaus, J.; Krzywinski, J.; Saldin, E.; Schneidmiller, E.; Yurkov, M. Regenerative FEL amplifier at the TESLA test facility at DESY. *Nucl. Instrum. Methods Phys. Res. Sect. A Accel. Spectrometers Detect. Assoc. Equip.* **1999**, *429*, 424–428. [CrossRef]
29. Huang, Z.; Ruth, R.D. Fully Coherent X-ray Pulses from a Regenerative-Amplifier Free-Electron Laser. *Phys. Rev. Lett.* **2006**, *96*, 144801. [CrossRef]
30. Freund, H.P.; van der Slot, P.J.M.; Shvyd'ko, Y. An X-ray regenerative amplifier free-electron laser using diamond pinhole mirrors. *New J. Phys.* **2019**, *21*, 093028. [CrossRef]
31. Trovò, M.; Clarke, J.; Couprie, M.; Dattoli, G.; Garzella, D.; Gatto, A.; Giannessi, L.; Günster, S.; Kaiser, N.; Marsi, M.; et al. Operation of the European storage ring FEL at ELETTRA down to 190 nm. *Nucl. Instrum. Methods Phys. Res. Sect. A Accel. Spectrometers Detect. Assoc. Equip.* **2002**, *483*, 157–161. [CrossRef]
32. Gandhi, P.; Penn, G.; Reinsch, M.; Wurtele, J.; Fawley, W. Oscillator seeding of a high gain harmonic generation free electron laser in a radiator-first configuration. *Phys. Rev. Spec. Top. Accel. Beams* **2013**, *16*, 020703. [CrossRef]
33. Li, K.; Yan, J.; Feng, C.; Zhang, M.; Deng, H. High brightness fully coherent x-ray amplifier seeded by a free-electron laser oscillator. *Phys. Rev. Accel. Beams* **2018**, *21*, 040702. [CrossRef]
34. Petrillo, V.; Bacci, A.; Rossi, A.R.; Serafini, L.; Drebot, I.; Conti, M.R.; Ruijter, M.; Opromolla, M.; Samsam, S.; Broggi, F.; et al. Coherent, high repetition rate tender X-ray Free-Electron Laser seeded by an Extreme Ultra-Violet Free-Electron Laser Oscillator. *New J. Phys.* **2020**, *22*, 073058. [CrossRef]
35. Mirian, N.; Opromolla, M.; Rossi, G.; Serafini, L.; Petrillo, V. High-repetition rate and coherent free-electron laser in the tender x rays based on the echo-enabled harmonic generation of an ultraviolet oscillator pulse. *Phys. Rev. Accel. Beams* **2021**, accepted.

36. Newnam, B.E. Extreme ultraviolet free-electron laser-based projection lithography systems. *Opt. Eng.* **1991**, *30*, 1100–1108. [CrossRef]
37. Penco, G.; Perosa, G.; Allaria, E.; Di Mitri, S.; Ferrari, E.; Giannessi, L.; Spampinati, S.; Spezzani, C.; Veronese, M. Enhanced seeded free electron laser performance with a "cold" electron beam. *Phys. Rev. Accel. Beams* **2020**, *23*, 120704. [CrossRef]
38. Beye, M. *FLASH2020+: Making FLASH Brighter, Faster and More Flexible : Conceptual Design Report*; Verlag Deutsches Elektronen-Synchrotron: Hamburg, Germany, 2020; pp. 1–126. [CrossRef]
39. Reiche, S. GENESIS 1.3: A fully 3D time-dependent FEL simulation code. *Nucl. Instrum. Methods Phys. Res. Sect. A Accel. Spectrometers Detect. Assoc. Equip.* **1999**, *429*, 243–248. [CrossRef]
40. Faatz, B.; Plönjes, E.; Ackermann, S.; Agababyan, A.; Asgekar, V.; Ayvazyan, V.; Baark, S.; Baboi, N.; Balandin, V.; von Bargen, N.; et al. Simultaneous operation of two soft x-ray free-electron lasers driven by one linear accelerator. *New J. Phys.* **2016**, *18*, 062002. [CrossRef]
41. Rossbach, J.; Schneider, J.R.; Wurth, W. 10 years of pioneering X-ray science at the Free-Electron Laser FLASH at DESY. *Phys. Rep.* **2019**, *808*, 1–74. [CrossRef]
42. Nölle, D. FEL Operation at the European XFEL Facility. In Proceedings of the International Free Electron Laser Conference (FEL'19), Hamburg, Germany, 26–30 August 2019; Number 39 in International Free Electron Laser Conference; JACoW: Geneva, Switzerland, 2019; [CrossRef]
43. Liu, T.; Dong, X.; Feng, C. Start-to-end Simulations of the Reflection Hard X-Ray Self-Seeding at the SHINE Project. In Proceedings of the FEL'19, Geneva, Switzerland, 26–30 August 2019; Number 39 in Free Electron Laser Conference; pp. 254–257. [CrossRef]
44. Hemsing, E.; Marcus, G.; Fawley, W.M.; Schoenlein, R.W.; Coffee, R.; Dakovski, G.; Hastings, J.; Huang, Z.; Ratner, D.; Raubenheimer, T.; et al. Soft X-ray seeding studies for the SLAC Linac Coherent Light Source II. *Phys. Rev. Accel. Beams* **2019**, *22*, 110701. [CrossRef]
45. Reiche, S. Overview of Seeding Methods for FELs. In Proceedings of the 4th International Particle Accelerator Conference, Shanghai, China, 12–17 May 2013.
46. Xie, M. Design optimization for an X-ray free electron laser driven by SLAC LINAC. *Conf. Proc.* **1996**, *C950501*, 183–185. [CrossRef]
47. Hemsing, E.; Stupakov, G.; Xiang, D.; Zholents, A. Beam by design: Laser manipulation of electrons in modern accelerators. *Rev. Mod. Phys.* **2014**, *86*, 897–941. [CrossRef]
48. Guenster, S.; Ristau, D.; Gatto, A.; Kaiser, N.; Trovo, M.; Danailov, M.; Sarto, F. VUV Optics Development for the Elettra Storage Ring FEL. In Proceedings of the 26th International Free Electron Laser Conference & 11th FEL Users Workshop, Trieste, Italy, 29 August–3 September 2004.
49. Henke, B.; Gullikson, E.; Davis, J. X-ray Interactions: Photoabsorption, Scattering, Transmission, and Reflection at E = 50-30,000 eV, Z = 1-92. *At. Data Nucl. Data Tables* **1993**, *54*, 181–342. Available online: https://henke.lbl.gov/optical_constants/mirror2.html (accessed on 10 May 2021). [CrossRef]
50. Agapov, I.; Geloni, G.; Tomin, S.; Zagorodnov, I. OCELOT: A software framework for synchrotron light source and FEL studies. *Nucl. Instrum. Methods Phys. Res. A* **2014**, *768*, 151–156. [CrossRef]
51. Oepts, D.; van der Meer, A.; van Amersfoort, P. The Free-Electron-Laser user facility FELIX. *Infrared Phys. Technol.* **1995**, *36*, 297–308. [CrossRef]
52. Jaroszynski, D.; Oepts, D.; Van Der Meer, A.; Van Amersfoort, P.; Colson, W. Consequences of short electron-beam pulses in the FELIX project. *Nucl. Instrum. Methods Phys. Res. Sect. A Accel. Spectrometers Detect. Assoc. Equip.* **1990**, *296*, 480–484. [CrossRef]
53. Knippels, G.M.H.; Bakker, R.J.; van der Meer, A.F.G.; Jaroszynski, D.A.; Oepts, D.; van Amersfoort, P.W.; Hovenier, J.N. Dynamic cavity desynchronisation in FELIX. *Nucl. Instrum. Methods Phys. Res. A* **1994**, *341*, ABS26–ABS27. [CrossRef]
54. MacLeod, A.M.; Yan, X.; Gillespie, W.A.; Knippels, G.M.H.; Oepts, D.; van der Meer, A.F.G.; Rella, C.W.; Smith, T.I.; Schwettman, H.A. Formation of low time-bandwidth product, single-sided exponential optical pulses in free-electron laser oscillators. *Phys. Rev. E* **2000**, *62*, 4216–4220. [CrossRef]
55. Zhao, Z.Y.; Li, H.T.; Jia, Q.K. Effect of cavity length detuning on the output characteristics for the middle infrared FEL oscillator of FELiChEM. *Chin. Phys. C* **2017**, *41*, 108101. [CrossRef]
56. Kiessling, R.; Colson, W.B.; Gewinner, S.; Schöllkopf, W.; Wolf, M.; Paarmann, A. Femtosecond single-shot timing and direct observation of subpulse formation in an infrared free-electron laser. *Phys. Rev. Accel. Beams* **2018**, *21*, 080702. [CrossRef]
57. Vinokurov, N.A.; Skrinsky, A.N. *About the Maximum Power of an Optical Klystron on a Storage Ring*; Report No. BINP 77-67; Budker Institute for Nuclear Physics: Novossibirsk, Russia, 1977.
58. Dattoli, G.; Giannessi, L.; Ottaviani, P. MOPA optical klystron FELs and coherent harmonic generation. *Nucl. Instrum. Methods Phys. Res. Sect. A Accel. Spectrometers Detect. Assoc. Equip.* **2003**, *507*, 26–30. [CrossRef]
59. Penco, G.; Allaria, E.; Ninno, G.D.; Ferrari, E.; Giannessi, L. Experimental Demonstration of Enhanced Self-Amplified Spontaneous Emission by an Optical Klystron. *Phys. Rev. Lett.* **2015**, *114*, 013901. [CrossRef]
60. Penco, G.; Allaria, E.; De Ninno, G.; Ferrari, E.; Giannessi, L.; Roussel, E.; Spampinati, S. Optical Klystron Enhancement to Self Amplified Spontaneous Emission at FERMI. *Photonics* **2017**, *4*, 15. [CrossRef]
61. Ding, Y.; Emma, P.; Huang, Z.; Kumar, V. Optical klystron enhancement to self-amplified spontaneous emission free electron lasers. *Phys. Rev. ST Accel. Beams* **2006**, *9*, 070702; Erratum in **2020**, *23*, 019901. [CrossRef]

62. Geloni, G.; Guetg, M.; Serkez, S.; Schneidmiller, E. A Revision of Optical Klystron Enhancement Effects in SASE FELs. *Phys. Rev. Accel. Beams*. **2021**, submitted.
63. Keil, B.; Baldinger, R.; Ditter, R.; Gloor, M.; Koprek, W.; Marcellini, F.; Marinkovic, G.; Roggli, M.; Rohrer, M.; Stadler, M.; et al. Status of The European XFEL Transverse Intra Bunch Train Feedback System. In Proceedings of the International Beam Instrumentation Conference (IBIC2015), Melbourne, Australia, 13–17 September 2015; Number 4 in International Beam Instrumentation Conference; JACoW: Geneva, Switzerland, 2016; pp. 492–496. [CrossRef]
64. Obier, F.; Decking, W.; Hüning, M.; Wortmann, J. Fast Kicker System for European XFEL Beam Distribution. In Proceedings of the 39th International Free-Electron Laser Conference, Hamburg, Germany, 26–30 August 2019; JACoW Publishing: Geneva, Switzerland, 2019; p. 4. [CrossRef]